Current and Emerging Diagnostic Imaging-Based Techniques for Assessment of Osteoporosis and Fracture Risk

Anu Shaju Areeckal, *Student Member, IEEE*, Michel Kocher, and Sumam David S., *Senior Member, IEEE*

(Methodological Review)

***Abstract*—Osteoporosis is a metabolic bone disorder characterized by low bone mass, degradation of bone microarchitecture, and susceptibility to fracture. It is a growing major health concern across the world, especially in the elderly population. Osteoporosis can cause hip or spinal fractures that may lead to high morbidity and socio-economic burden. Therefore, there is a need for early diagnosis of osteoporosis and prediction of fragility fracture risk. In this review, state of the art and recent advances in imaging techniques for diagnosis of osteoporosis and fracture risk assessment have been explored. Segmentation methods used to segment the regions of interest and texture analysis methods used for classification of healthy and osteoporotic subjects are also presented. Furthermore, challenges posed by the current diagnostic tools have been studied and feasible solutions to circumvent the limitations are discussed. Early diagnosis of osteoporosis and prediction of fracture risk require the development of highly precise and accurate low-cost diagnostic techniques that would help the elderly population in low economies.**

***Index Terms*—Diagnostic radiography, fracture risk prediction, image segmentation, image texture analysis, medical diagnostic imaging, osteoporosis.**

I. Introduction

OSTEOPOROSIS is a bone condition caused by reduction in bone mass and degeneration of bone structure, which leads to high susceptibility of fragility fractures. Osteoporosis-related fracture is a major global health risk, affecting one in three women and one in five men over the age of 50. According to the Asia-Pacific Regional Audit in 2013, osteoporosis accounts for more hospitalization than diabetes, myocardial infarction, and breast cancer in women above the age of 45 [1]. It is more prevalent among the elderly population, especially postmenopausal women [2]. As the aging population increases, so will the incidence of fractures. It is projected that by 2050, at least one-third of the world population will be aged over 50 years, and in Asia alone, a 7.6-fold increase in ageing population is expected, that may result in more than 50% of the global fractures to occur in Asia [1].

Osteoporosis is a silent disease, being painless and asymptomatic and is often undiagnosed until a fragility fracture occurs. After an initial fracture, there is a high risk for subsequent fractures [3]. The risk of osteoporotic fracture is 40% to 50% for women and 13% to 22% for men [4], and fragility fractures could increase the morbidity and mortality of the affected people. The mortality rate associated with hip fracture is about 15% to 20% [5]. Of those affected, about 50% suffer permanent disabilities and about 20% fatalities; only 30% recover fully [6]. Studies and therapeutical practices in osteoporosis treatment have shown that this bone condition can be cured if it is diagnosed before the occurrence of the first fragility fracture [7]. This calls for an urgent need for highly accurate, sensitive, and low-cost techniques for early diagnosis of osteoporosis and prediction of fracture risk.

Progression of osteoporosis can be assessed by measuring different properties of weight-bearing bones. Human bone consists of two components: first, cortical bone, which is compact and forms the outer covering of tubular bones; and second, trabecular or cancellous bone, which has a spongy appearance and is found in the inner regions of tubular bones. Osteoporosis causes thinning of cortical bones and deterioration of the trabecular bone network. Since trabecular bone undergoes changes in bone characteristics earlier than cortical bone during the onset of osteoporosis, measurements of trabecular bone would give a more sensitive measurement and could help in early diagnosis of osteoporosis [8]. Quantitative imaging techniques have been developed for quantification of bone density and architecture for the diagnosis of osteoporosis and monitoring of therapeutical interventions. Even though there exists biochemical markers measured using blood and urine samples, (e.g., osteocalcin, urinary hydroxyproline, bone-specific alkaline phosphatase, C-terminal collagen telopeptide, collagen crosslinks, etc.) that can give information on bone formation and resorption

Manuscript received January 10, 2018; revised April 19, 2018; accepted June 26, 2018. Date of publication July 3, 2018; date of current version February 15, 2019. *(Corresponding author: Anu Shaju Areeckal.)*

A. S. Areeckal and S. David S. are with the Department of Electronics and Communication Engineering, National Institute of Technology Karnataka, Surathkal 575025, India (e-mail: anu_shaju_ec13f06@nitk.edu.in; sumam@ieee.org).

M. Kocher is with the Department des Technologies Industrielles, Haute Ecole d'Ingenierie et de Gestion du Canton de Vaud (HEIG-VD), Yverdon-les-Bains CH-1401, Switzerland (e-mail: michel.kocher@heig-vd.ch).

Digital Object Identifier 10.1109/RBME.2018.2852620

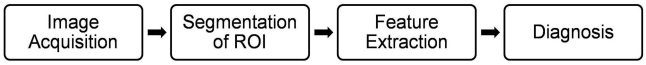

Fig. 1. Pipeline of a diagnostic technique to detect osteoporosis.

for the measurement of changes in bone mineral density (BMD) and fracture risk, they are not widely used in clinical practice due to biological and analytical variabilities [9], [10]. Quantitative imaging techniques are widely used due to their high precision and reproducibility and validation on a large number of population studies. The aim of this paper is to review the current and emerging imaging-based diagnostic tools for detection of osteoporosis and prediction of fragility fracture risk. A literature survey included the databases, IEEE *Xplore*, PubMed, Science Direct, Wiley, and SpringerLink. Articles published during 2000–2018 and significant articles published earlier were included in this survey.

The diagnostic imaging-based tools used for detection of osteoporosis follows a general pipeline with mainly four stages: 1) image acquisition, 2) segmentation of region-of-interest (ROI), 3) feature extraction, and 4) diagnosis (as shown in Fig. 1). In the first stage, images are acquired using dedicated imaging modalities. The bone ROI is then segmented from the image using manual, semiautomated, or automated techniques in stage 2. In stage 3, various measurements of the cortical and/or trabecular bone characteristics are extracted from the segmented ROI and used to provide a diagnosis of the severity of osteoporosis and risk of fracture. In stage 4, a diagnostic decision is made either using T- and Z-scores calculated from normal reference values or using supervised learning techniques for classification of subjects into healthy or osteoporotic group. The subsequent four sections discuss in detail about each of the four stages. Section II details the quantitative imaging techniques developed for diagnosis of osteoporosis and Section III presents the segmentation methods used for segmenting the bone regions from the images acquired. Section IV describes the different feature extraction methods used to quantify bone density and architecture from the bone ROI and Section V explains how these features are used for diagnostic decision making. Tools developed for the prediction of future risk of fragility fracture are presented in Section VI. Section VII discusses the challenges of the existing diagnostic techniques and future directions for research.

II. Quantitative Imaging Techniques Used for Diagnosis of Osteoporosis

Osteoporosis is a systemic disease affecting the whole skeletal body. Different imaging modalities are being used for the diagnosis of osteoporosis. The earliest noninvasive diagnostic techniques include measurement of cortical thickness and radiolucency from radiographs. Absorptiometric techniques later developed brought a standardized measurement of bone loss for the diagnosis of osteoporosis. These techniques measure bone density of mainly the hip, lumbar spine, or forearm, as these weight-bearing bones are highly susceptible to fragility fractures. Other quantitative imaging techniques have been developed for volumetric quantification of bone architecture. Due to higher metabolic activity of trabecular bone, texture analysis of trabecular-rich skeletal sites give a more sensitive measurement. This section discusses the current and emerging quantitative imaging techniques used for the diagnosis of osteoporosis.

A. Dual X-Ray Absorptiometry (DXA)

The gold standard for diagnosis of osteoporosis is the determination of BMD using DXA [11]. DXA uses two X rays of different energies, a high-energy beam (>70 keV) and a low-energy beam (30–50 keV), to scan the bone region [12]. Soft tissue subtraction is employed by taking the difference between absorption of the two X-ray energies by the bone region to produce a DXA image of the bone. The ROI is automatically segmented from the DXA image and the bone mineral content (BMC) of the ROI is measured. BMD is obtained as the ratio of BMC to the total area of the ROI and is measured as g/cm^3. The measured BMD of a patient is compared with reference BMD value of young healthy gender-matched adult reference population having peak bone mass. T-score is calculated as the standard deviation of the measured BMD from the reference BMD. As recommended by the World Health Organization (WHO), osteoporosis is diagnosed based on the T-scores: T-score ≥ -1 indicates normal BMD, T-score ≤ -2.5 indicates osteoporosis, and T-score between -1 and -2.5 indicates osteopenia or low bone mass. T-score ≤ -2.5 accompanied by a fragility fracture denotes severe osteoporosis [11].

The skeletal sites commonly used for measurement are the hip and lumbar spine using central DXA and the forearm using peripheral DXA. DXA measurements at different skeletal sites give different values of BMD. Usually the lowest BMD value obtained is considered for the diagnosis. Fracture risk assessed from central DXA gives a more accurate value than that of forearm, as these skeletal sites are more susceptible to osteoporotic fractures, and hence, the central DXA is the preferred choice for clinical trials.

DXA has a high precision (maximum acceptable precision error of 2%–2.5%), low radiation exposure (1–50 millisievert (mSv)) and a short scanning time [12]. DXA–BMD is accurate and can explain 70% of the bone strength. Major limitations of DXA in low economies are its high cost and limited availability. DXA gives an areal measurement of BMD and is sensitive to variations in bone size. Moreover, BMD alone is not a good determinant of the risk of fragility fractures. This limitation can be circumvented by the use of volumetric quantification techniques that measure the trabecular bone.

B. Quantitative Computed Tomography (QCT)

QCT is a widely used technique that gives a volumetric measurement of the trabecular bone density. In QCT, X-ray attenuation by tissues is captured at different angles across the ROI. A phantom with different bone densities is placed near the patient during acquisition, so that the attenuation measured in Hounsfield units can be converted into BMD values measured in milligrams hydroxyapatite per cubic centimeter. The images are obtained as slices of the scanned region and a three-dimensional (3-D) model is reconstructed from the slices. Since the

attenuation coefficients of cortical and trabecular bones are different, they can be easily separated. QCT is used to measure the trabecular bone density at the spine and hip. Use of a calibration standard is important to produce consistent results across CT scanners from different manufacturers.

QCT gives a true volumetric measurement of BMD independent of the body size. Measurement of trabecular bone density gives a more sensitive measurement compared to DXA–BMD. QCT can also better diagnose patients with obesity and degenerative diseases. Trabecular BMD measured by QCT at the total femur can predict hip fractures as good as DXA–BMD of the hip in older men and women. However, QCT has a high cost of scan and high radiation dose (0.06–2.9 mSv). Artifacts during image acquisition can tamper the QCT image, reducing the accuracy of measurement.

T-scores obtained from QCT are lower than that of DXA, and hence, cannot be analyzed using the WHO classification of osteoporosis. Instead, the volumetric BMD values can be used to measure fracture risk with 110–80 mg/cm^3 denoting mild increase, 80–50 mg/cm^3 amounting to moderate increase, and $<$50 mg/cm^3 representing severe increase in fracture risk [12]. QCT scan of the proximal femur can be projected into a 2-D image that can be analyzed to determine DXA equivalent values [13]. This technique is called computed tomography X-ray absorptiometry (CTXA). Areal CTXA values can be used with WHO classification and for fracture risk assessment tool (FRAX) score determination. Dual-energy QCT helps to increase the accuracy of BMD measurements as compared to single-energy QCT [14]. Micro-CT captures details of both cortical and trabecular bone microstructure at a very high resolution of 1–100 μm^3 and is highly correlated with bone histomorphometric analysis. Multidetector CT (MDCT) offers higher spatial resolution than spiral CT scanners. MDCT features of the distal tibia is well correlated with micro-CT derived features [15]. Even though MDCT gives a highly accurate measurement of bone density, this spatial resolution is not sufficient to image trabecular bone architecture. High-resolution MDCT requires higher radiation dose of approximately 3 mSv [12]. Recently, an ultralow-dose MDCT with 50%, 25%, and 10% of the original dose was investigated [16]. Density and microstructure features extracted using MDCT were able to differentiate between healthy and vertebral fractured groups.

C. High-Resolution Peripheral QCT (HR-pQCT)

HR-pQCT is a QCT technique that acquires high-resolution volumetric images of the peripheral parts of the body, such as distal radius and tibia. The ROI is semiautomatically segmented using edge detection to detect the boundary of the bone region. Cortical bone compartment is segmented using Gaussian smoothing filter and thresholding method. Trabecular bone is obtained by removing the cortical bone from total bone region. HR-pQCT can simultaneously measure both bone density and bone architecture of the trabecular and cortical bones. A calibration phantom is used to measure volumetric BMD similar to QCT. Different morphometric analyses are done to analyze the connectivity and anisotropy of the bone architecture. Finite element analysis can also be performed on the HR-pQCT image and biomechanical properties of the trabecular bone can be measured.

High-resolution imaging provides very fine details of the cortical and trabecular architecture. HR-pQCT has a higher resolution, signal-to-noise ratio, and lower radiation dose than MDCT. HR-pQCT density measurements have a high reproducibility with coefficient of variation $<1\%$. The 3-D structural parameters measured by pQCT are highly correlated with that of micro-CT with coefficient of determination, $R^2 > 0.9$.

Due to peripheral measurement, it is convenient for morbid patients or those suffering from a spinal or hip fracture. Bone density and microstructural measurements of pQCT can predict osteoporosis independently of DXA [17], [18]. HR-pQCT is able to measure differences in bone microarchitecture of individuals with identical BMD values [19], [20]. A limitation of pQCT is the necessity of registration of follow-up scans with a high accuracy in the order of 100 μm for longitudinal studies. This is a difficult task due to the long acquisition time and introduction of artifacts by even the slightest movement of the limb.

D. Quantitative Ultrasound (QUS)

QUS is a simple cost-effective radiation-less technique for measurement of trabecular bone architecture. QUS uses pulsed sound waves to propagate through the bone, with frequency range (500 kHz–1.25 MHz). It measures bone properties based on differential reflections and attenuation of sound waves. The bone properties are characterized by two measurements, namely, broadband ultrasound attenuation (BUA) and speed of sound (SOS). BUA increases and SOS decreases with osteoporosis. Other measurements taken from QUS, such as stiffness index, QUS index, amplitude-dependent SOS, and apparent integrated backscatter can help in identifying patients with high fracture risks. Dedicated QUS scanners are available for calcaneum, phalanx, and tibia. Of these, the calcaneal QUS devices are the most accurate and widely explored for texture analysis.

Population studies have shown the ability of QUS to discriminate between people with and without osteoporotic fractures [21]–[23]. Calcaneal QUS can predict hip and major osteoporotic fracture in older men and women, independent of DXA–BMD measurement. QUS has the advantage of no radiation, low cost, portability of equipment, measurement at the peripheral limb, etc. However, QUS measurements vary with different manufacturers and for different skeletal sites. Calcaneal QUS has a poor correlation with DXA of hip and spine. Hence, device-specific diagnostic thresholds are predefined by calibrating QUS measurements with DXA [24]. Other drawbacks of QUS are low precision and lack of sensitivity [25]. QUS has a poor reliability and reproducibility due to improper placing of transducers and variations in temperature. This limits its use as a clinical diagnostic tool for osteoporosis but useful as a prescreening tool.

E. Magnetic Resonance Imaging (MRI)

MRI is a nonionizing modality that helps in volumetric analysis of trabecular bone. MRI takes advantage of diffusive water present in the porous geometry of trabecular bone architecture. From the MRI images, trabecular bone region is segmented and histomorphometric features, such as thickness and connectivity of the trabecular structure, is analyzed. Even though MRI is promising for monitoring osteoporosis, it is still not commonly used in clinical practice. Limitations of MRI are long scan time and susceptibility to partial volume effects and motion artifacts. Susceptibility artifacts in MRI can amplify the size of the trabecular bone network, and thus, affect morphometric measurements.

High-resolution micro-MRI (HR micro-MRI) is being explored for the study of trabecular bone structure [26]. HR-MRI may be imaged at 1.5 or 3.0 T. The limitation of imaging at 1.5 T is low SNR and spatial resolution. The trabecular features obtained from HR-MRI is highly correlated with that of pQCT. Strength of the cortical and trabecular bone can also be assessed by quantifying the relaxometry properties of the adjoining bone marrow using quantitative magnetic resonance (QMR) and adiposity of bone marrow using proton MR spectroscopy (MRS). MRS can give information on the water and fat content and different compartments of lipids in the bone marrow. Bone marrow perfusion indices measured using dynamic contrast-enhanced MRI can be used as a biomarker for bone quality assessment. An inverse proportionality exists between bone marrow fat and BMD, and a direct proportionality between bone marrow perfusion indices and BMD [12].

F. Digital X-Ray Radiogrammetry (DXR)

DXR is a combined computerized radiogrammetry and texture analysis technique used for the measurement of BMD [27]. It was introduced as a cost-effective alternative to DXA, useful for low economies. DXR uses a single-hand radiograph to estimate BMD from the three middle metacarpal bones. The ROI is automatically segmented from the hand image using active shape model segmentation method. A combined radiogrammetric measurement of the cortical bone (MCI) and textural analysis (cortical porosity index) is used to obtain bone volume per area, which is then scaled by a constant in order to be approximated to DXA–BMD at the forearm.

DXR–BMD shows a good correlation to DXA–BMD values of forearm, hip, and spine. However, the BMD measured by DXR is not a true volumetric measure of bone density. DXR does not account for the texture analysis of trabecular bone architecture that could provide a more sensitive measurement.

G. Radiography

Although all the quantitative imaging techniques being developed for diagnosis of osteoporosis are precise and promising, most of these techniques, such as DXA, QCT, HR-pQCT, MRI, etc., have high cost of scans and low availability in most developing countries, which limits its use for mass screening for osteoporosis and follow-up examinations during therapeutical treatments. To circumvent this limitation, radiography has gained attention due to its low cost, wide availability, and ease of acquisition. With the advancement of high-processing computers, many studies are being done to employ advanced image processing and machine learning techniques for assessment of osteoporosis and fracture risk using radiographs only. Radiographs of weight-bearing bones such as hip, lumbar spine, calcaneum, forearm, and dental radiographs are usually used. The bone ROIs are manually or automatically segmented. Features extracted from the radiographs include radiogrammetry, texture analysis for information on connectivity, anisotropy, etc. Supervised learning techniques are then used to train classifier models for discrimination of osteoporotic from healthy people. These methods will be discussed in detail in the following sections.

Table I summarizes the current techniques used for diagnosis of osteoporosis.

III. Segmentation Methods

Diagnostic approaches employing texture analysis of radiographs mostly use manual segmentation of the ROI by experts. Manual segmentation is time consuming and produces high intraobserver and interobserver variabilities. So it is essential to develop standardized automated segmentation methods for segmentation of bone ROIs that reduce subjective error and are robust to noise and varying acquisition conditions. This section discusses various automated segmentation methods used for segmentation of ROIs in the diagnostic techniques for osteoporosis. The segmentation methods can be broadly grouped as edge detection methods, region growing methods, deformable models, and deep learning methods.

A. Edge Detection Methods

Edge-based segmentation methods include edge detectors, such as Sobel and Robert operators, Canny edge detection, gradient detection, Laplace operators, etc. Edge detectors help in detecting discontinuities in gray-level intensities. They are usually used as a preprocessing tool to enhance the edges of the ROI and help in increasing the accuracy of segmentation methods. Edge detection algorithms have been employed for the segmentation of femur bones and lumbar vertebra for the diagnosis of osteoporosis [28], [29].

B. Region Growing Methods

Region growing algorithm is a simple and efficient segmentation method where a seed point is placed manually or automatically inside the ROI and a homogenous region is grown around the seed point.

Watershed segmentation is a hybrid region growing method where images are thought of as topographic surfaces and water is flood from the local minima to fill up catchment basins. Watershed lines created to separate the catchment basins form the boundary of the ROI [30]. Watershed segmentation has been used for the segmentation of metacarpal bones using medial axis transform and showed high inter- and intraobserver

TABLE I
SUMMARY OF CURRENTLY AVAILABLE IMAGING-BASED DIAGNOSTIC TECHNIQUES FOR OSTEOPOROSIS

Diagnostic tool	ROI	Features extracted	Significance	Limitations
DXA	Lumbar spine, hip, forearm, whole body	BMD is measured as the ratio of BMC and area	Gold standard, Low radiation exposure	Expensive, Not widely available in developing economies, Measures areal BMD, Does not account for details on bone structure
QCT	Lumbar spine and hip	Volumetric BMD using a calibration phantom	Provides a volumetric BMD, Sensitive due to measurements from trabecular bone	Expensive, Higher radiation dose than DXA
pQCT	Distal radius and tibia	Cortical and trabecular density and architecture	Ease of convenience due to peripheral measurement, Convenient due to peripheral measurement	Expensive, High radiation dose
QUS	Calcaneum, phalanx, tibia and radius	Sound attenuation and velocity	No radiation involved, Low cost, Portable device	Poor precision and sensitivity, Poor reproducibility
MRI	Forearm, hip and spine	Histomorphometric measures	No radiation involved, Provides a volumetric measurement	Expensive
DXR	Metacarpal bones of hand	BMD is derived from radiogrammetry and cortical porosity	No subjective human error, Good correlation with DXA	Does not measure true volumetric BMD, Trabecular texture not taken into account

agreement of 92% and 96%, respectively [31]. The main disadvantage of conventional watershed method is oversegmentation due to the presence of noise in the image. This can be overcome by placing markers to even out the local minima due to noise and watershed segmentation is done with these markers as local minima. Marker-controlled watershed segmentation has been used to segment third metacarpal bone for measurement of cortical radiogrammetry [32], [33]. This method showed mean absolute error of 0.2 and 0.17 mm in the measurement of metacarpal cortical thickness of healthy subjects and subjects with low bone mass, respectively [33]. Marker-controlled watershed segmentation of wavelet decomposed images has been used for the segmentation of trabecular bone in micro-CT images [34]. This technique showed lower segmentation error as compared to other approaches.

C. Deformable Models

The different types of deformable model-based segmentations are Active Contour Models or Snakes, Active Shape Model (ASM), Active Appearance Model (AAM), etc.

Active contour, also known as Snakes, is a segmentation method in which an initial curve is moved within an image to find object boundaries [35]. It is a deformable spline that tries to minimize the energy function under the constraints of forces that pull the curve towards the edges while resisting deformations. It requires a prior knowledge of the shape of object so that the initial curve can be placed appropriately. An adaptive contour segmentation was proposed to automatically segment cortical and trabecular bones in CT images of vertebra and tibia [36]. Recently, Independent Active Contour Segmentation was introduced for the segmentation of trabecular bone in micro-CT images [37]. It is a two-step process where ROIs are extracted automatically using heuristic thresholding and image patching and independent instances of active contour is applied to each ROI.

ASM is a parametric deformable model in which prior shape information of the object is utilized. A mean shape model of the object is generated from a large annotated set of training images. Principal component analysis is used to describe the variations in object in the training data [38]. ASM has been used to automatically segment ROI from radiographic images. DXR took 103 training images for the ASM model of metacarpal and obtained a reconstruction success of 99.5% on 5000 test images [39]. A fully automated deformable model was developed to segment phalanx from hand radiographs [40]. The average Hausdorff distance achieved was 5.6 pixels. A modified ASM was proposed for segmentation of distal radius in DXA images, which increased the segmentation accuracy of conventional ASM-based method by 47.4% [41].

AAM is a robust segmentation method that combines shape and texture information of the object [42]. AAM is computationally more expensive than ASM. AAM has been used for the segmentation of hand bones, vertebra, etc., for the diagnosis of osteoporosis [43], [44].

D. Deep Learning Methods

Convolutional neural network (CNN) is a deep neural network where the input can be given in the form of images. Many layers of convolutional and pooling stages help to extract the complex details in images with fewer parameters, and hence, is easier to train. CNN architectures have been recently used for segmentation of femur from MR images [45]. Two architectures were explored, namely, a pyramidal CNN and a u-net CNN architecture and a high dice score of 0.95 was obtained. Deep neural networks can perform much better than other state-of-the-art segmentation methods, but it requires a large amount of training data for achieving robustness and high accuracy.

Table II shows the advantages and disadvantages of different segmentation methods used in diagnostic techniques for the segmentation of ROIs for detection of osteoporosis.

IV. FEATURE EXTRACTION METHODS

Following image acquisition and segmentation of the bone regions, the next step is to extract features from the ROI that can best capture the properties of the bone. The features extracted

TABLE II
SEGMENTATION METHODS USED IN DIAGNOSTIC TECHNIQUES

Segmentation methods	Advantages	Disadvantages
Watershed [30]	Simple and easy implementation Does not require any training data	Sensitive to noise in the image Accuracy depends on the contrast of object boundary to background
Active Contour [35]	Placement of initial contour helps in a guided segmentation	Accuracy depends on proper placement of initial contour
ASM [38]	High accuracy, precision and reliability Robust to noise and illumination conditions	Requires a large training set for high accuracy Manual annotation of training data is time consuming
AAM [42]	More accurate and robust than ASM	Computationally more expensive than ASM
CNN [45]	Achieves a very high accuracy	Requires a large training dataset

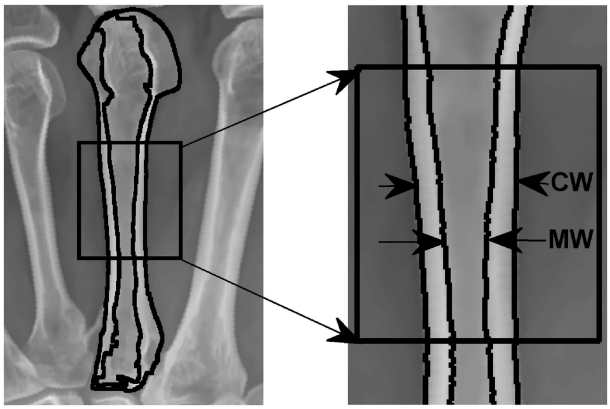

Fig. 2. Radiogrammetry of metacarpal bone of hand [46].

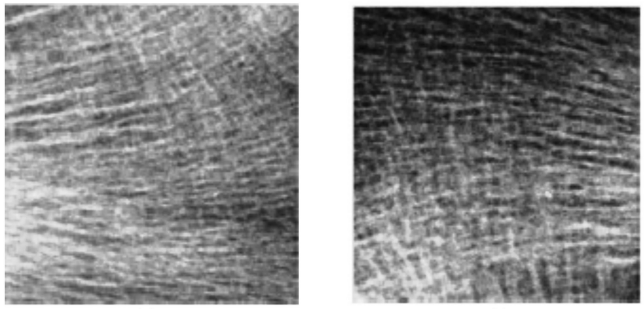

Fig. 3. Texture analysis of trabecular bone of (a) healthy and (b) osteoporotic bone [49].

can be grouped as radiogrammetry, bone density, and texture analysis.

A. Radiogrammetric Measurements

Manual radiogrammetry is one of the earliest diagnostic techniques by which the dimensions of bones are measured by using caliper from radiographs. Measurements taken using radiogrammetry of cortical bone are cortical width (CW), medullary width, cortical area, length of bone, etc., as shown in Fig. 2 [46]. From these radiogrammetric measurements, various bone indices are formulated. Some of the popular bone indices derived from radiogrammetric measurements include Barnett and Nordin Index (BNI), biconcavity index, combined cortical thickness (CCT), metacarpal Index (MCI), Exton–Smith Index, pediatric bone index (PBI), etc. [47], [48].

Although manual radiogrammetry provided a simple and inexpensive method for evaluating bone loss, it suffered from subjective errors. Automating the radiogrammetric technique increase the accuracy, precision, and reproducibility of the measurements. Threshold values are determined for the radiogrammetric indices in order to distinguish between osteoporotic and nonosteoporotic groups. An automated radiogrammetric method for classification of healthy people and people with low bone mass was recently developed using hand radiographs [43]. This method takes radiogrammetric measurements from third metacarpal bone of hand and uses these features to train different classifier models. The extracted radiogrammetric indices showed a high significance of $p < 0.001$ using independent sample *t* test and a good correlation with DXA–BMD of lumbar spine. Hence, computerized radiogrammetry of radiographs can be used as a low-cost tool for screening people for low bone mass.

B. Bone Density Measurement

Measurement of BMD is the most commonly used method for diagnosis of osteoporosis in clinical practice. Quantitative imaging techniques like DXA, QCT, and DXR measure the BMD from the segmented bone regions of the acquired images. As discussed in Section II, DXA measures BMD as the ratio of BMC to the area of ROI. In QCT, a calibration phantom is used to convert the attenuation of X-rays measured in Hounsfield units to BMD values. DXR combines MCI and cortical porosity indices and converts it into DXA-equivalent BMD values.

Measurement of bone density cannot accurately predict the risk of fracture in people as it is a measurement of bone quantity alone. Osteoporosis is also characterized by bone quality, i.e., the deterioration of bone architecture. Quantification of trabecular bone architecture can give a sensitive measurement for the early diagnosis of osteoporosis. This can be done with the help of texture analysis methods as discussed in the next section.

C. Texture Analysis

Texture analysis methods are currently being explored for characterization of trabecular bone of calcaneum, proximal femur, lumbar vertebra, distal radius, dental images, etc., as these bone regions have a high content of trabecular network. The texture features extracted are then used with supervised learning techniques to discriminate between healthy and osteoporotic fractured groups. Fig. 3 shows the texture of trabecular bone in calcaneal radiographs of healthy and osteoporotic bones [49].

Feature extraction methods used for texture analysis of trabecular bone can be broadly grouped as: 1) trabecular pattern indices, 2) histomorphometric analysis, 3) fractal analysis, 4) statistical analysis, 5) structural analysis, and 6) transform-based analysis. These methods are explained briefly below.

1) Trabecular Pattern Indices: Trabecular pattern indices were originally developed to analyze the pattern of trabecular bone region from radiographs for detection of bone loss. Three popular trabecular pattern indices that analyze trabecular bone in calcaneal, proximal femur, and vertebra are Calcaneal Index, Singh Index, and Saville Index, respectively.

Tensile and compression trabeculae present in calcaneal bone are uniformly distributed in a healthy bone. Tensile trabeculae degrade faster than compression trabeculae during progression of osteoporosis. These anisotropic variations occurring in calcaneal bone texture is analyzed by a five-grade calcaneal index [50]. The five-grade calcaneal index was later modified to a three-grade modified calcaneal index that significantly correlated with BMD of hip and distal radius and QUS measurements [51].

Singh Index is a grading system based on patterns in proximal femur radiographs [52]. A set of reference radiographs of six grades were created by analyzing the tensile and compressive trabeculae. The proximal femur radiographs to be analyzed are compared with the reference radiographs and categorized to the grade that best represented the trabecular pattern.

Saville Index was used to detect osteoporosis by the analysis of trabecular patterns in spinal radiographs [53]. It analyzes the end plates and striations present in the vertebra and classifies it into five grades. Due to the high subjective error caused by manual assessment of radiographs, these trabecular pattern indices are seldom used in clinical practice.

2) Histomorphometric Analysis: The reduction in trabecular network due to osteoporosis can be analyzed using connectivity analysis. Trabecular connectivity can be measured by histomorphometric analysis using computerized morphometry, node-strut analysis, star-volume analysis, etc. [54]–[57].

Features measured using computerized histomorphometric analysis include trabecular area, perimeter, number, thickness, separation, ratio of bone volume to tissue volume, etc. Node-strut analysis analyzes the interconnections in a trabecular bone network obtained after a skeletonization process. Features extracted using node-strut analysis are the number of nodes per tissue volume, ratio of node length to termini length, etc. Other histomorphometric features extracted include marrow star volume that estimates the mean size of the marrow space, trabecular bone pattern factor that measures the convexity in bone structure, index of interconnectivity, Euler number, etc.

3) Fractal Analysis: Fractal analysis has been widely explored for trabecular bone texture analysis. Fractal analysis measures the roughness or irregularity of objects based on self-similar subobjects. The structural organization of bone is more anisotropic for the osteoporotic cases than healthy subjects. Fractal analysis of bone radiographs using directional average method, box counting method, variance method, etc., have been employed [58], [59]. Features extracted by fractal analysis are fractal dimension (FD), H parameter, and fractal signature. Fractal parameters are significantly different in the healthy and osteoporotic groups. Fractal analysis is able to detect significant differences in bone texture that showed similar BMD values [60]. An FD is correlated with the porosity of 3-D microarchitecture of trabecular bone and helps to quantify changes in 3-D trabecular structure [61].

4) Statistical Analysis: Statistical methods characterize texture by measuring the distribution and relationship between pixel intensity values of an image. Gray Level Co-occurrence Matrix (GLCM) is a second-order statistical method that defines how many times a pixel pair co-occurs within a given distance and direction [62]. The matrix is constructed at orientations 0^0, 45^0, 90^0, and 135^0 for a fixed distance. Texture features such as energy, contrast, correlation, homogeneity, etc., are calculated from the resulting four matrices. GLCM features have been extracted from calcaneal and dental images for the evaluation of osteoporosis. GLCM features from 2-D images are correlated with the 3-D bone microarchitectural parameters [63].

Gray-level run length matrix (GLRLM) is a higher-order statistical method that represents the number of adjacent pixels having the same gray values along a particular direction [64]. Some of the important features extracted from GLRLM are short run emphasis and long run emphasis that measures the distribution of short and long runs and gray-level nonuniformity and run-length nonuniformity that measures the similarity of gray-level intensities and run lengths throughout the image. Fine textures have more short runs with similar intensities. GLRLM features can significantly discriminate healthy subjects from people with low bone mass [46].

5) Structural Analysis: Structural methods describe the texture primitives and their spatial arrangements. Commonly used structural methods are gradient-based methods, Laws' masks, local binary pattern (LBP), etc.

Mathematical morphology can be used to extract features that are invariant under linear grayscale transformations. Mathematical morphological gradients originally developed with bone texture images using different structuring elements were found to be superior to gray-level dependence matrix, Fourier and fractal methods for discriminating between healthy and osteoporotic groups [65].

Laws' texture masks are filter masks built from the combination of five 1-D kernel vectors [66]. These five 1-D kernels used are level vector, edge vector, spot vector, ripple vector, and wave vector, that measure the average intensity, gradient, spot, ripple, and changes in gray-level values, respectively. The variance of each feature is computed over a moving window that provides local texture energy. Laws' masks and statistical measures have been used for bone texture analysis in osteoporosis [67]. The best discriminating ability was obtained by the combination of edge and average graylevel Laws' masks.

LBP is a widely explored feature extraction method that combines both statistical and structural texture features. LBP describes texture through statistical distribution of local patterns, obtained by labeling image pixels by thresholding the neighborhood of each pixel with its intensity value. LBP histograms of texture images can be compared to classify healthy and

osteoporotic groups. Statistical features can also be extracted from LBP histograms to form feature vectors. A 3-D LBP helps in describing local changes in the 3-D bone structure during progression of osteoporosis [68].

6) Transform-Based Analysis: Transform-based methods make use of different transforms such as Fourier and Wavelet transforms to extract texture features. Fast Fourier transform (FFT) features enhance the high-frequency contents in the image and have been used to characterize trabecular bone texture. New anisotropy indices were derived from FFT to assess the degree of anisotropy on calcaneal radiographs and achieved better performance than that of BMD of lumbar spine, femoral neck, and total femur [69], [70].

Wavelet transform decomposes a texture image by filtering consecutively along horizontal and vertical directions with low-pass and high-pass filters. This produces four subimages that represent a lower resolution of the original image, enhanced vertical edges, enhanced horizontal edges, and enhanced diagonal edges of the image, respectively. Every subimage contains information of a specific scale and orientation and have different energies that can be extracted to obtain the feature vector.

Gabor filter is a local bandpass filter that analyzes the frequency content of texture images in particular directions in localized regions. By filtering an image with Gabor filters of different orientations and spatial frequencies, different sets of coefficients are obtained that represents the feature vector of the texture. Gabor features extracted from proximal femur radiographs are correlated with the corresponding Singh index and with central DXA [71], [72].

V. Approaches to Diagnostic Decision Making

The final step of the diagnostic tool pipeline is diagnostic decision making to detect osteoporosis using the extracted features. There are two following approaches to this: first, comparison with a reference value to detect osteoporosis, and second, using supervised learning techniques to train classifiers to classify healthy and osteoporotic subjects.

A. Comparison With a Reference Value

Most diagnostic techniques using radiogrammetric and bone density measurements use this approach for diagnosing osteoporosis. As discussed in Section IV, radiogrammetric indices use a reference threshold value to diagnose osteoporosis. As bone characteristics vary with gender and ethnicity, the reference threshold values could vary when measured on a population different from the one originally studied. Fixing this threshold reference relies on studies conducted on a large sample population matched for gender and ethnicity.

DXA uses a reference BMD of Caucasian women of age 20–29 years to calculate T-score of the measured BMD of a subject [11]. The diagnosis of osteoporosis using T-score is recommended by WHO for postmenopausal women and men above the age of 50 years. The International Society of Clinical Densitometry guidelines recommend calculation of Z-scores using an age and gender-matched reference population for premenopausal women and men below the age of 50 years [73]. Z-score ≤ -2 indicates the presence of osteoporosis.

B. Supervised Learning Techniques

Machine learning techniques can be used to train classifiers using the extracted features to classify osteoporotic cases from healthy controls. Some commonly used classifiers are support vector machine (SVM), *K*-nearest neighbor (KNN), random forest (RF), artificial neural network (ANN), etc. SVM is a nonparametric classifier that builds a hyper plane in a higher dimensional feature space for classification. KNN is a simple nonparametric method by which an object is classified by assigning it to the class most common among its KNN. RF classifies the image by applying majority voting to the classes predicted by individual decision tree classifiers. ANN is a data-driven self-adaptive technique whose performance depends on the network architecture and number of inputs. Deep network architecture has many layers of neurons and trained weights that help to extract complex features from input data for the classification of images into various classes. The performance of the trained classifiers can be evaluated using confusion matrix, from which different metrics, such as sensitivity (Sn), specificity (Sp), precision and accuracy (Acc), etc., are derived. Receiver operating characteristic (ROC) curve is a plot of true positive rate versus false positive rate whose area, AUC, gives a measure of how well a classifier is able to classify into positive or negative class. Another useful evaluation metric is Odd's Ratio (OR), which is defined as the ratio of the odds that an outcome will occur in the presence of an exposure to the odds of the outcome occurring in its absence. The remaining section reviews research work that used supervised learning techniques to train classifiers in order to distinguish between normal controls and osteoporotic cases.

1) Techniques Based on Radiogrammetry: Radiogrammetric measurements are usually used to diagnose osteoporosis using a cutoff threshold value. Computerized radiogrammetric indices have been used to train classifiers using machine learning techniques to detect people with low bone mass [43]. Radiogrammetric indices such as CCT, BNI, and PBI were measured from the third metacarpal bone of hand radiographs and four classifiers were trained, namely, KNN, SVM, decision tree, and ANN. The best performance results was observed using ANN classifier with a test accuracy of 74.1%.

A limitation of the computerized radiogrammetry is that it does not account for the bone structure, which decreases the accuracy of classification. Our recent study used cortical radiogrammetric measurement of third metacarpal bone along with trabecular texture analysis of distal radius from hand and wrist radiographic images for detection of low bone mass in people [46]. Classifier trained with the combination of the most significant cortical and trabecular bone features helped to increase the classification accuracy of test data to 88.5%, as compared to test accuracy of 73.3% obtained using a classifier trained with cortical features alone. Kathirvelu and Anburajan [74] combined cortical bone thickness and trabecular area of the mandible along with age to diagnose osteoporosis from dental radiographs. Their method achieved a good accuracy of 84%

with sensitivity of 92% and positive predictive value of 85%. Combination of CW measurement of the mandibular cortex and texture features based on FD and GLCM in dental panoramic radiographs showed a higher performance of AUC = 0.872 and sensitivity and specificity of 80%, than using CW alone [75].

2) Techniques Based on Density Measurements: Bone density measurements alone are not sufficient to accurately predict the risk of fractures, and hence, trabecular texture features are included to train classifiers to detect susceptibility to osteoporotic fractures. Assessment of vertebral fracture along with BMD has been shown to enhance fracture risk prediction [76]. Combination of BMD with texture parameters from Fourier and fractal methods produced better results (AUC of 0.82) than using BMD only (AUC of 0.78) and texture parameters only (AUC of 0.72) [77]. Benhamou *et al.* [78] showed that addition of low H_{mean} fractal measure to BMD of lumbar spine increased the OR of fracture from 6.1 to 9.0 OR of fracture for combined femoral neck BMD and low H_{mean} parameter was observed to be 14.06, while that for femoral neck BMD alone is 4.78 [79]. Touvier *et al.* [59] showed the potential interest of the combination of BMD, spinal TBS, and calcaneal H parameter to discriminate patients with and without osteoporotic fractures.

3) Techniques Based on Texture Analysis: Texture analysis of the trabecular bone are being studied at the calcaneum, hip, lumbar vertebra, distal radius, dental radiographs, etc., as these skeletal sites contain a high percentage of trabecular bone. Studies on texture analysis of calcaneal and dental radiographs are the most widely explored work. The feature extraction methods used to analyze the texture of trabecular bone using calcaneal and dental radiographs and their performance results are given in Table III. As seen in the table, classifiers trained on calcaneal radiographs in recent studies show a high performance in discriminating between osteoporotic cases and healthy controls and are thus promising.

Although a few attempts of deep learning with radiographs of trabecular bone regions for diagnosis of osteoporosis have been done in recent years, the trained deep classifiers failed to give a good accuracy [93], [94]. This could be due to the use of a very small dataset for training. Training deep classifiers with a sufficiently large dataset could help in the extraction of high-level features that can detect even small changes due to bone loss and thus help in an early diagnosis of osteoporosis.

VI. Prediction of Fracture Risk

Assessment of risk factors for osteoporotic fracture and its prognosis is an emerging and challenging research area. Very few techniques exist currently for the prediction of fracture risk in clinical practice, such as Trabecular Bone Score (TBS), FRAX, etc.

A. Trabecular Bone Score

TBS is a texture analysis method that analyze the bone texture of DXA images of lumbar spine [95]. TBS is used to predict fracture risk by computing mean variations in two pixel intensities with a separation vector. A high TBS value indicates dense microarchitecture of bone with well-connected trabeculae. TBS $>$ 1.35 is normal and TBS $<$ 1.20 indicates degraded microstructure. The values in between this range represent partial degradation of microstructure. TBS is correlated with microarchitectural features measured from micro-CT, such as bone volume fraction, number and separation of trabeculae, etc. [96]. Several work have been done recently to explore the clinical utility of TBS in population studies. TBS can predict osteoporotic fractures in postmenopausal women and men above the age of 50 years [97]. TBS can be used with FRAX and BMD to adjust FRAX fracture risk in older men and women [73].

B. Fracture Risk Calculators (FRC)

The major risk factors of osteoporosis-related fractures are age, gender, ethnicity, body weight, early menopause, low exercise, prolonged immobility or sedentary lifestyle, poor nutrition (Calcium, Vitamin D, and proteins), prolonged intake of alcohol, caffeine and tobacco, medications such as glucocorticoids, benzodiazepines, anticonvulsants, thyroid hormones, etc., recent falls, prior fragility fracture, and family history of osteoporotic fractures especially at the hip. FRCs have been developed using risk factors to predict the risk of future fragility fractures. Table IV details the fracture risk models developed for prediction of fracture risk based on risk factors.

1) FRAX: FRAX is a 10-year fracture risk assessment tool released in 2008 [98]. It was developed from 9 population-based cohorts and validated on 11 population-based cohorts. It predicts the risk of fracture quantitatively by taking into account the DXA–BMD measured at the femoral neck as well as clinical risk factors. When DXA–BMD measurement is not available, FRAX predicts the risk of fracture using clinical risk factors alone, which may not give an accurate and precise prognosis. FRAX can underestimate fracture risk in patients with recent fracture [103]. It has a high negative predictive value and low positive predictive value, compared to other fracture risk tools [104].

2) FORE FRC: FORE FRC is very similar to FRAX except that FORE FRC will show higher fracture rates in women with shorter life expectancy [99]. Unlike FRAX, FORE FRC categorizes fracture risk as low, medium, and high risk. FORE FRC also gives a graphical presentation of the fracture risk for an easy interpretation of the results.

3) QFracture: QFracture is a fracture risk calculator, developed for the UK population [100]. In addition to the risk factors considered in FRAX, QFracture takes into account a detailed medical history that is routinely documented during clinical trials [105]. QFracture is a better hip fracture risk predictor than FRAX [104].

4) Garvan: Garvan calculator was developed from the Dubbo Osteoporosis Epidemiology Study (DOES) of Australian population [101]. In comparison to FRAX and QFracture, Garvan calculator considers very few risk factors, namely, age, gender, previous history of fracture, and fall, with an optional BMD value or weight. Garvan calculator is found to overestimate major osteoporotic fracture risk as compared to FRAX [106].

TABLE III
TRABECULAR TEXTURE ANALYSIS USING RADIOGRAPHS

No.	Texture Analysis and Classification	ROI	Performance Results	Dataset	Reference
1	Proposed an interconnectivity index, NDX, using trabecular and node-strut features, SVM classifier	Calcaneal	Acc of 94.36%	71 women with 11 healthy, 19 osteopenic, 31 OP and 10 severely OP cases	[80]
2	Dual-tree transform M-band on projected image with Renyi entropy and divergence, KNN classifier	Calcaneal	Acc of 98%	39 fractured cases and 38 controls	[81]
3	GLCM, RLM features from variational decomposition of image	Calcaneal	Acc of 85%	87 fractured cases and 87 controls	[82]
4	One dimensional LBP on projected and enhanced image	Calcaneal	Acc of 71.3% and AUC of 91%	39 fractured cases and 41 controls	[83]
5	Gabor filter bank, discrete wavelet frames, fractal dimension, LBP, discrete Fourier and Cosine transforms, Laws masks, edge histogram and GLCM, Bayes-Naive classifier	Calcaneal	Acc of 79.3% and AUC = 81%	58 OP cases and 58 controls	[84]
6	Wavelet decomposition and parametric circular models	Calcaneal	AUC = 96.5%	87 fractured cases and 87 controls	[85]
7	New anisotropic Discrete Dual Tree Wavelet Transform, SVM classifier	Calcaneal	Sn=90%, Sp=93%, Acc = 91%	87 fractured cases and 87 controls	[86]
8	First and second order statistical features trained on SVM, KNN, Naive Bayes, ANN classifiers	Calcaneal	For SVM: Sn=100%, Sp=95.74%, Acc = 97.87%	87 fractured cases and 87 controls	[87]
9	Mandibular cortical width, FD, GLCM with RF classifier	Dental	AUC=0.872, Sn=Sp=80%	663 women with 140 OP cases and 523 controls	[75]
10	CCT, mandibular trabecular area, age	Dental	Acc = 84%, Sn = 92%, PPV = 85%, AUC=0.89	36 OP cases and 28 controls	[74]
11	Proposed Mandibular Cortical degree, SVR (Support Vector Regression)	Dental	AUC = 0.88	12 OP cases, 18 osteopenic and 69 controls	[88]
12	Fractal, radiogrammetric and histomorphometric analysis of mandibular bone, GSF (Genetic Swarm Fuzzy) classifier	Dental	Sn=99.1%, Sp=98.4%, Acc = 98.9% using hip BMD	141 women with 20 OP and 121 controls as per hip BMD	[89]
13	Histogram of Gradients (HoG) features, SVM classifier	Dental	Acc = 72.5%	19 OP cases and 21 controls	[90]
14	Fourier power spectrum-based fractal analysis	DR	OR=1.5 comparable to trabecular BMD	30 OP cases and 27 controls	[91]
15	Fractal, histomorphometric and skeletal measures, SVM classifier	DR	Max Sn = 79% and Sp = 66%	47 OP cases and 47 controls	[92]
16	Metacarpal radiogrammetry, GLRLM, Laws' masks, ANN classifier	DR	Acc = 88.5%	71 OP cases and 67 controls	[46]

DR-Distal Radius, Acc- Accuracy, AUC- Area Under ROC curve, Sn- Sensitivity, Sp- Specificity, OR- Odd's Ratio, OP- Osteoporotic

TABLE IV
FRACTURE RISK PREDICTION MODELS

Fracture risk model	Inclusion criteria	Clinical risk factors	Outcome	Weblink
FRAX	Men and women aged 40-90 years	Age, gender, ethnicity, weight, height, history of previous fracture, parental history of fractured hip, smoking and drinking habits, use of glucocorticoids, presence of rheumatoid arthritis or secondary osteoporosis.	10 year probability of a hip fracture and a major osteoporotic fracture, with or without BMD measurement	[98]
FORE FRC	Postmenopausal women and men aged 45 years or more and not receiving treatment for osteoporosis	Age, gender, ethnicity, weight, height, history of previous fracture, parental history of fractured hip, smoking and drinking habits, use of glucocorticoids, presence of rheumatoid arthritis or secondary osteoporosis.	10 year probability of a hip fracture and a major osteoporotic fracture, with BMD measurement	[99]
QFracture	Men and women aged 30-99 years	Age, gender, ethnicity, weight, height, history of previous fracture, parental history of fractured hip, smoking and drinking habits, use of glucocorticoids, antidepressants, steroids or estrogen, presence of rheumatoid arthritis, secondary osteoporosis, diabetes, dementia, cancer, asthma, stroke, chronic liver or kidney disease, Parkinsons disease, epilepsy, malabsorption and endocrine problems.	1 to 10 year probability of a hip fracture and a major osteoporotic fracture without BMD measurement	[100]
Garvan	Men and women aged 50-96 years	Age, gender, weight, history of previous fracture.	5 and 10 year probability of a hip fracture and a major osteoporotic fracture, with or without BMD measurement	[101]
Fracture Index	Men and women of all ages	Age, weight, maternal history of fracture, smoking habit, use of arms to stand up from a sitting position, and BMD T-score.	5 year non- vertebral, vertebral and hip fracture risks with and without BMD T- score measurement	[102]

TABLE V
AVAILABILITY OF IMAGING MODALITIES USED FOR OSTEOPOROSIS IN DIFFERENT COUNTRIES [1], [4], [108]–[110]

Country	DXA*	CT*	MRI*
USA	35.80 (2003)	41.86 (2016)	36.72 (2016)
Japan	20.80 (2013)	107.12 (2014)	51.67 (2014)
France	29.10 (2010)	16.94 (2016)	13.54 (2016)
Germany	21.10 (2010)	35.09 (2015)	33.63 (2015)
Australia	18.00 (2013)	63.17 (2016)	14.34 (2016)

*Units are in number of devices per million population (Year)

5) FRACTURE Index: FRACTURE Index was developed from the Study of Osteoporotic Fractures (SOF) data and validated on the Epidemiology of Osteoporosis (EPIDOS) data [107]. It can be used with or without BMD T-score to predict five year risk of hip, vertebral, and nonvertebral fracture risks [102].

VII. DISCUSSION AND FUTURE DIRECTIONS

This section discusses the limitations of the current diagnostic tools and possible solutions that could help to circumvent them.

A. Usage and Quality Control

DXA suffers from issues regarding usage and quality control. Often the automatically segmented images of DXA is not accurate and needs to be corrected manually by a trained technician. The presence of osteoarthrosis, scoliosis, and previous fracture can be detected on the DXA scans and should be excluded. This requires a trained technician and rigorous quality control [11]. Quality control of DXA requires periodic scanning of a calibration phantom and system maintenance using the manufacturer guidelines. A cross-calibration of DXA machines is essential during replacement of old machines, to facilitate quantitative comparison to the previous DXA machine. All quantitative imaging techniques require regular quality control and device-specific training is necessary for the technicians prior to clinical use. Also, prospective trials of different modalities should be conducted for independent validation for fracture risk prediction.

B. Cost and Availability

Table V shows the availability of imaging modalities in different countries [1], [4], [108]–[110]. In India, DXA costs from 27 to 67 USD and QUS costs between 25 to 40 USD [1]. Being expensive, DXA machines are not widely available in low economies. In India, the number of DXA machines available per 1 million of its population is 0.26. This urges the need for low cost alternatives for diagnosis of osteoporosis in developing countries. A cost effective method for the diagnosis would be a combined approach using low-cost imaging modalities accounting for both reduction in bone mass and structure. This can be achieved through a combination of densitometric, radiogrammetric, and texture analysis of the cortical and trabecular bone.

C. Measurement

DXA–BMD is an areal measurement and does not give a true volumetric density of bone. Areal measurement of bone density can overestimate BMD in people with low stature or those having osteoarthritis in the hip or spine. It can also underestimate BMD in obese people and patients with degenerative bone diseases like osteomalacia. Quantitative imaging techniques, such as QCT, pQCT, and MRI, can measure volumetric bone density but are quite expensive.

Texture characterization of trabecular bone helps to improve the sensitivity of the detection of osteoporosis. The use of high resolution imaging modalities like HR-pQCT, micro-CT, HR-MRI, micro-MRI, etc., which can capture the fine detail of bone structure proves to be promising in this direction. Trabecular texture features need to be further validated with larger datasets from different population before its use in clinical practice.

D. Integration of Monomodal and Multimodal Features

Combining the features of different quantitative imaging techniques could give a more accurate diagnosis and prediction. But the combined approach may not be feasible as it results in a higher cost and radiation dose from the multiple scans. A solution could be to use a high-resolution quantitative imaging technique and employ advanced image processing and texture analysis techniques for a better prediction. Deep learning could be a promising solution for the identification of stronger features that can detect early changes in bone due to osteoporosis. But this requires a very large image dataset that should be specific to a particular ethnic group and gender.

Use of different feature extraction methods, such as radiogrammetric measurements and texture analysis in images obtained from the same quantitative imaging technique, would be helpful in providing a better diagnosis and prediction without additional radiation exposure and cost of scans. As an example, radiogrammetric measurements of the hip from DXA images are found to associated with hip fracture risk [73]. TBS, which is a texture analysis method of the spinal DXA images, is promising for the prediction of hip and major osteoporotic fractures. Hence, using DXA imaging alone, densitometric, radiogrammetric, and texture analysis could be combined together to give a better prognosis of fracture risk.

Another solution to a better prediction would be to combine features extracted from other tissues adjoining the bone that also undergo changes due to osteoporosis. For example, quantification of bone marrow adiposity and perfusion are found to be potential biomarkers for assessment of the bone quality. Studies based on this are being done using QMR, MRS, and dynamic contrast-enhanced MRI.

E. Improving Fracture Risk Prediction

FRAX tool can predict fracture risk in men and women among a large number of population from different countries. However, the existing fracture risk scores are determined from

only the DXA–BMD values and/or clinical parameters, such as demographic and anthropometric details and behavioral habits. These scores do not include all the known risk factors and bone textural characteristics which could be highly potential for the assessment of fragility fracture risk. Assessment of fracture risk using bone texture characterization along with BMD is crucial for a precise and sensitive measurement of risk of future fractures. Also, FRAX does not consider the dose response of the clinical risk factors used. Inclusion of dose response of risk factors such as intake of alcohol and drugs, etc., will give an improved prediction of fracture risk.

Recent studies have investigated other potential clinical risk factors for osteoporotic fracture, such as insulin-dependent diabetes mellitus, height loss since age 25 years, use of antidepressants, history of myocardial infarction or angina, hyperthyroidism, etc. [111]–[113]. Iron Deficiency Anemia is an independent risk factor of osteoporosis [114]. Presence of multiple morbidities is observed to have a high risk of hip fracture [113]. Sarcopenia along with osteoporosis is a good predictor of hip fracture [115]. Decreased sleep quality and later sleep timing are reported to be risk factors for low bone mass and sarcopenia [116]. A promising direction for further improvement of prognosis of fracture risk is the combination of biochemical markers, that are known to be associated with bone loss, with clinical risk factors and quantitative imaging features of bone density and microarchitecture. This requires validation on prospective trials. In a recent study, genetic profiling of BMD-associated genetic variants along with clinical risk factors was reported to increase the accuracy of fracture prediction [117]. Hence, prediction of fracture risk is an open area of research.

F. Need for a Reference Standard and Database

Different imaging modalities measuring different sites yield different measurement values. For example, bone density measurements of the hip, spine, and forearm of the same patient gives different BMD values and T-scores. Each skeletal site have different bone densities and rates of bone loss. Use of different ROIs can give different fracture risk predictions. This discrepancy makes the diagnosis and fracture risk assessement difficult. Thus, a reference standard is essential for the quantitative imaging modalities. For diagnosis using DXA, the reference standard recommended by WHO is the BMD measured at femoral neck [11].

WHO recommends use of NHANES-III database containing the BMD measurements of Caucasian women to be used as reference for women and men of all ethnic groups [11]. However, bone characteristics and the mean reference BMD value vary among men and women and among different ethnic groups. Thus, BMD measurement using DXA with young Caucasian women as the reference standard may overestimate or underestimate the BMD values for other ethnic groups. There is a lack of databases containing adequate observations for other ethnic groups. Moreover, different manufacturers of DXA use different reference databases that show different BMD values for the same patient at the same site of measurement. These values have to be converted to standardized BMD values for follow-up studies or for comparison with others. There is a need for standardization of reference databases used in commercial densitometric devices that are matched for gender and ethnicity.

Multicenter prospective cohort databases being studied for the analysis of fracture risks include SOF, DOES, EPIDOS, Os des Femmes de Lyon (OFELY), Swiss Evaluation of the Methods of Measurement of Osteoporotic Fracture Risk (SEMOF), Osteoporotic Fractures in Men (MrOS), Basel Osteoporosis Study, Framingham Osteoporosis Study, National Osteoporosis Risk Assessment, EPISEM, etc. [118]–[125]. Texture Characterization of Bone is a public dataset of 174 calcaneal radiographic images, that was part of the IEEE-ISBI Challenge 2014 [49].

The prime hindrance to the advancement of research being held in detection of osteoporosis and assessment of fracture risks is the lack of availability of a publicly available large dataset for research work. Even though there are various studies being conducted on the development of better diagnostic tools for osteoporosis and fracture risk, the data used is either not publicly available or is not large enough to be used for advanced techniques like machine learning. Therefore, there is a need for building a large database for population studies on osteoporosis and fracture risks and for the development of advanced diagnostic tools with high accuracy and precision. The database being built should include demographic, anthropometric, and clinical parameters of the volunteers. Additional information on biochemical markers and genetic profiling using blood and urine samples will be helpful. DXA of the femoral neck and lumbar spine should be acquired for comparison of the developed tool with the gold standard. Along with DXA, TBS measured using spinal DXA image and FRAX score measured using DXA–BMD should be recorded. As for texture analysis, HR-pQCT or high-resolution radiography images can be acquired. pQCT is preferable as it gives a volumetric measurement. Calcaneal QUS measurements can also be recorded as it will not contribute to additional radiation. The imaging techniques used must follow a standard protocol and should be done with different devices across multicenters in order to remove any device or operator-dependent bias in measurements. The volunteers must be followed up atleast once in every two years and the parameters discussed above needs to stored. This will help in an efficient longitudinal study of fracture risks. Different databases must be created for different ethnic groups, as the bone characteristics and measurement variables vary with ethnicity. However, cost factors also needs to be considered. It would be difficult for the volunteers, especially the older individuals in developing economies, to bear the expenses of all these tests. Building a large database would require the help of a funding agency.

G. Conclusion

In conclusion, the current techniques used for diagnosis of osteoporosis and fracture risk prediction have been discussed. Even though the gold standard technique for diagnosis of osteoporosis, DXA, is accurate and highly precise, it suffers from certain limitations, such as high cost and low availability of DXA in low economies. Diagnosis of osteoporosis from analysis of radiographs can be a cost-effective alternative to

DXA. Since BMD measures the bone quantity and not the bone structure, it is insufficient to predict the risk of fragility fracture. Texture analysis of the trabecular bone gives a measure of the microstructural architecture of the bone. Also, onset of osteoporosis impacts the trabecular bone architecture earlier than the cortical bone. Hence, a combination of bone density measurement with the trabecular bone texture analysis can give a more sensitive measure for early detection of osteoporosis. Moreover, DXA gives an areal BMD. Though QCT and MRI techniques give a true volumetric bone density, they are quite expensive. Hence, new low-cost diagnostic tools that measure a true volumetric bone density and also characterize the trabecular bone texture need to be investigated, in order to give a more accurate, sensitive, and reliable measurement for diagnosis of osteoporosis and prediction of fracture risk. This could pave way to remarkable advancements in clinical trials useful for both clinicians and elderly patients in future.

Acknowledgment

The authors would like to thank the Department of Orthopedics, Kasturba Medical College Hospital, Mangalore, Manipal Academy of Higher Education, Karnataka, India, and the Department of Radiology and Medical Informatics, University Hospital of Geneva, Geneva, Switzerland.

References

[1] IOF, "Asia-Pacific regional audit on epidemiology, costs and burden of osteoporosis in 2013," IOF Regionals 4th Asia-Pacific Osteoporosis Meeting, Hong Kong, Tech. Rep. 201311-1500, 2013.

[2] N. D. Nguyen, H. G. Ahlborg, J. R. Center, J. A. Eisman, and T. V. Nguyen, "Residual lifetime risk of fractures in women and men," *J. Bone Mineral Res.*, vol. 22, no. 6, pp. 781–788, 2007.

[3] J. R. Center, D. Bliuc, T. V. Nguyen, and J. A. Eisman, "Risk of subsequent fracture after low-trauma fracture in men and women," *JAMA*, vol. 297, no. 4, pp. 387–394, 2007.

[4] O. Johnell and J. Kanis, "Epidemiology of osteoporotic fractures," *Osteoporosis Int.*, vol. 16, no. 2, pp. S3–S7, 2005.

[5] L. J. Melton, "Who has osteoporosis? A conflict between clinical and public health perspectives," *J. Bone Mineral Res.*, vol. 15, no. 12, pp. 2309–2314, 2000.

[6] World Health Organization, "Chronic rheumatic conditions,." (2016). [Online]. Available: http://www.who.int/chp/topics/rheumatic/en/

[7] N. C. Harvey *et al.*, "Mind the (treatment) gap: A global perspective on current and future strategies for prevention of fragility fractures," *Osteoporosis Int.*, vol. 28, no. 5, pp. 1507–1529, 2017.

[8] J. E. Adams, "Quantitative computed tomography," *Eur. J. Radiol.*, vol. 71, no. 3, pp. 415–424, 2009.

[9] H. W. S. Cabral *et al.*, "The use of biomarkers in clinical osteoporosis," *Revista da Associação Médica Brasileira*, vol. 62, no. 4, pp. 368–376, 2016.

[10] A. Looker *et al.*, "Clinical use of biochemical markers of bone remodeling: Current status and future directions," *Osteoporosis Int.*, vol. 11, no. 6, pp. 467–480, 2000.

[11] J. A. Kanis, E. V. McCloskey, H. Johansson, A. Oden, L. J. Melton, and N. Khaltaev, "A reference standard for the description of osteoporosis," *Bone*, vol. 42, no. 3, pp. 467–475, 2008.

[12] T. M. Link, "Osteoporosis imaging: state of the art and advanced imaging," *Radiology*, vol. 263, no. 1, pp. 3–17, 2012.

[13] A. D. Brett and J. K. Brown, "Quantitative computed tomography and opportunistic bone density screening by dual use of computed tomography scans," *J. Orthopaedic Transl.*, vol. 3, no. 4, pp. 178–184, 2015.

[14] A. Emami, H. Ghadiri, A. Rahmim, and M. Ay, "A novel dual energy method for enhanced quantitative computed tomography," *J Instrum.*, vol. 13, no. 1, 2018, Art. no. P01030.

[15] C. Chen *et al.*, "Quantitative imaging of peripheral trabecular bone microarchitecture using MDCT," *Med. Phys.*, vol. 45, no. 1, pp. 236–249, 2018.

[16] K. Mei *et al.*, "Is multidetector CT-based bone mineral density and quantitative bone microstructure assessment at the spine still feasible using ultra-low tube current and sparse sampling?" *Eur. Radiol.*, vol. 27, no. 12, pp. 5261–5271, 2017.

[17] H. Jiang, C. J. Yates, A. Gorelik, A. Kale, Q. Song, and J. D. Wark, "Peripheral quantitative computed tomography (pQCT) measures contribute to the understanding of bone fragility in older patients with low-trauma fracture," *J. Clin. Densitometry*, vol. 21, no. 1, pp. 140–147, 2018.

[18] C. Ohlsson *et al.*, "Cortical bone area predicts incident fractures independently of areal bone mineral density in older men," *J. Clin. Endocrinol. Metabolism*, vol. 102, no. 2, pp. 516–524, 2016.

[19] J. J. de Jong *et al.*, "Fracture repair in the distal radius in postmenopausal women: A follow-up 2 years postfracture using HRpQCT," *J. Bone Mineral Res.*, vol. 31, no. 5, pp. 1114–1122, 2016.

[20] G. J. Kazakia, A. J. Burghardt, T. M. Link, and S. Majumdar, "Variations in morphological and biomechanical indices at the distal radius in subjects with identical BMD," *J. Biomechanics*, vol. 44, no. 2, pp. 257–266, 2011.

[21] S. Fujiwara *et al.*, "Heel bone ultrasound predicts non-spine fracture in Japanese men and women," *Osteoporosis Int.*, vol. 16, no. 12, pp. 2107–2112, 2005.

[22] M. G. Gl *et al.*, "Prospective identification of postmenopausal osteoporotic women at high vertebral fracture risk by radiography, bone densitometry, quantitative ultrasound, and laboratory findings: Results from the PIOS study," *J. Clin. Densitometry*, vol. 8, no. 4, pp. 386–395, 2005.

[23] A. Diez-Perez *et al.*, "Prediction of absolute risk of non-spinal fractures using clinical risk factors and heel quantitative ultrasound," *Osteoporosis Int.*, vol. 18, no. 5, pp. 629–639, 2007.

[24] D. Hans, F. Hartl, and M. Krieg, "Device-specific weighted T-score for two quantitative ultrasounds: Operational propositions for the management of osteoporosis for 65 years and older women in Switzerland," *Osteoporosis Int.*, vol. 14, no. 3, pp. 251–258, 2003.

[25] C. Njeh *et al.*, "Comparison of six calcaneal quantitative ultrasound devices: Precision and hip fracture discrimination," *Osteoporosis Int.*, vol. 11, no. 12, pp. 1051–1062, 2000.

[26] F. W. Wehrli, "Structural and functional assessment of trabecular and cortical bone by micro magnetic resonance imaging," *J. Magn. Reson. Imag.*, vol. 25, no. 2, pp. 390–409, 2007.

[27] A. Rosholm, L. Hyldstrup, L. Baeksgaard, M. Grunkin, and H. Thodberg, "Estimation of bone mineral density by digital X-ray radiogrammetry: Theoretical background and clinical testing," *Osteoporosis Int.*, vol. 12, no. 11, pp. 961–969, 2001.

[28] P. Santhoshini, R. Tamilselvi, and R. Sivakumar, "Automatic segmentation of femur bone features and analysis of osteoporosis," *Lecture Notes Softw. Eng.*, vol. 1, no. 2, pp. 194–198, 2013.

[29] S. Ghosh, R. S. Alomari, V. Chaudhary, and G. Dhillon, "Automatic lumbar vertebra segmentation from clinical CT for wedge compression fracture diagnosis," *Proc. SPIE*, vol. 7963, 2011, Art. no. 796 303.

[30] F. Meyer, "Topographic distance and watershed lines," *Signal Process.*, vol. 38, no. 1, pp. 113–125, 1994.

[31] A. J. Raheja, "Automated analysis of metacarpal cortical thickness in serial hand radiographs," Master thesis, Dept. Biomed., Ind. Human Factors Eng., Wright State University, Dayton, OH, USA, 2008.

[32] A. S. Areeckal, S. S. David, M. Kocher, N. Jayasheelan, and J. Kamath, "Fully automated radiogrammetric measurement of third metacarpal bone from hand radiograph," in *Proc. IEEE Int. Conf. Signal Process. Commun.*, 2016, pp. 1–5.

[33] A. S. Areeckal, M. Sam, and S. S. David, "Computerized radiogrammetry of third metacarpal using watershed and active appearance model," in *Proc. IEEE 19th Int. Conf. Ind. Technol.*, 2018, pp. 1490–1495.

[34] W. A. Fourati and M. S. Bouhlel, "Trabecular bone image segmentation using iterative watershed and multi resolution analysis," *Int. J. Bio-Sci. Bio-Technol.*, vol. 3, no. 2, pp. 71–82, 2011.

[35] M. Kass, A. Witkin, and D. Terzopoulos, "Snakes: Active contour models," *Int. J. Comput. Vis.*, vol. 1, no. 4, pp. 321–331, 1988.

[36] M. Kovalovs and A. Glazs, "Trabecular bone segmentation by using an adaptive contour," *Rigas Tehniskas Universitates Zinatniskie Raksti*, vol. 14, pp. 6–11, 2013.

[37] V. Korfiatis, S. Tassani, and G. K. Matsopoulos, "An independent active contours segmentation framework for bone micro-CT images," *Comput. Biol. Med.*, vol. 87, pp. 358–370, 2017.

[38] T. F. Cootes, C. J. Taylor, D. H. Cooper, and J. Graham, "Active shape models- their training and application," *Comput. Vis. Image Understanding*, vol. 61, no. 1, pp. 38–59, 1995.

[39] H. H. Thodberg and A. Rosholm, "Application of the active shape model in a commercial medical device for bone densitometry," *Image Vis. Comput.*, vol. 21, no. 13, pp. 1155–1161, 2003.

[40] R. Dendere, G. Kabelitz, and T. S. Douglas, "Model-based segmentation of the middle phalanx in digital radiographic images of the hand," in *Proc. 35th Annu. Int. Conf. IEEE Eng. Med. Biol. Soc.*, 2013, pp. 3702–3705.

[41] S. Lee, S. Cho, and Y. M. Ro, "Enhanced distal radius segmentation in DXA using modified ASM," *IEICE Trans. Inf. Syst.*, vol. 94, no. 2, pp. 363–370, 2011.

[42] T. F. Cootes, G. J. Edwards, and C. J. Taylor, "Active appearance models," *IEEE Trans. Pattern Anal. Mach. Intell.*, vol. 23, no. 6, pp. 681–685, Jan. 2001.

[43] M. Sam, A. S. Areeckal, and S. S. David, "Early diagnosis of osteoporosis using active appearance model and metacarpal radiogrammetry," in *Proc. 13th Int. Conf. Signal-Image Technol. Internet-Based Syst.*, 2017, pp. 173–178.

[44] M. Roberts, T. F. Cootes, and J. E. Adams, "Vertebral morphometry: Semiautomatic determination of detailed shape from dual-energy X-ray absorptiometry images using active appearance models," *Investigative Radiol.*, vol. 41, no. 12, pp. 849–859, 2006.

[45] C. M. Deniz, S. Hallyburton, A. Welbeck, S. Honig, K. Cho, and G. Chang, "Segmentation of the proximal femur from MR images using deep convolutional neural networks," 2017, arXiv preprint arXiv:1704.06176.

[46] A. S. Areeckal, N. Jayasheelan, J. Kamath, S. Zawadynski, M. Kocher, and S. S. David, "Early diagnosis of osteoporosis using radiogrammetry and texture analysis from hand and wrist radiographs in Indian population," *Osteoporosis Int.*, vol. 29, no. 3, pp. 665–673, 2018.

[47] E. Barnett and B. Nordin, "The radiological diagnosis of osteoporosis: A new approach," *Clin. Radiol.*, vol. 11, no. 3, pp. 166–174, 1960.

[48] H. Thodberg, R. Van Rijn, T. Tanaka, D. Martin, and S. Kreiborg, "A paediatric bone index derived by automated radiogrammetry," *Osteoporosis Int.*, vol. 21, no. 8, pp. 1391–1400, 2010.

[49] TCB Challenge. [Online]. Available: www.univ-orleans.fr/i3mto/challenge-ieee-isbi-bone-texture-characterization

[50] N. Jhamaria, K. Lal, M. Udawat, P. Banerji, and S. Kabra, "The trabecular pattern of the calcaneum as an index of osteoporosis," *J. Bone Joint Surg.*, vol. 65, no. 2, pp. 195–198, 1983.

[51] K. Pande, S. Pande, D. de Takats, and E. McCloskey, "Modified calcaneal index: A new screening tool for osteoporosis based on plain radiographs of the calcaneum," *J. Orthopaedic Surg.*, vol. 13, no. 1, pp. 27–33, 2005.

[52] M. Singh, A. Nagrath, and P. Maini, "Changes in trabecular pattern of the upper end of the femur as an index of osteoporosis," *J. Bone Joint Surg.*, vol. 52, no. 3, pp. 457–467, 1970.

[53] P. D. Saville, "The syndrome of spinal osteoporosis," *Clinics Endocrinol. Metabolism*, vol. 2, no. 2, pp. 177–185, 1973.

[54] L. Dalle Carbonare *et al.*, "Bone microarchitecture evaluated by histomorphometry," *Micron*, vol. 36, no. 7, pp. 609–616, 2005.

[55] T. Tanaka, T. Sakurai, and I. Kashima, "Structuring of parameters for assessing vertebral bone strength by star volume analysis using a morphological filter," *J. Bone Mineral Metabolism*, vol. 19, no. 3, pp. 150–158, 2001.

[56] T. Schmah, N. Marwan, J. S. Thomsen, and P. Saparin, "Long range node-strut analysis of trabecular bone microarchitecture," *Med. Phys.*, vol. 38, no. 9, pp. 5003–5011, 2011.

[57] J. J. Hwang *et al.*, "Strut analysis for osteoporosis detection model using dental panoramic radiography," *Dentomaxillofacial Radiol.*, vol. 46, no. 7, 2017, Art. no. 20170006.

[58] R. Jennane, R. Harba, G. Lemineur, S. Bretteil, A. Estrade, and C. L. Benhamou, "Estimation of the 3D self-similarity parameter of trabecular bone from its 2D projection," *Med. Image Anal.*, vol. 11, no. 1, pp. 91–98, 2007.

[59] J. Touvier *et al.*, "Fracture discrimination by combined bone mineral density (BMD) and microarchitectural texture analysis," *Calcified Tissue Int.*, vol. 96, no. 4, pp. 274–283, 2015.

[60] K. Harrar and R. Jennane, "Trabecular texture analysis using fractal metrics for bone fragility assessment," *Int. J. Biomed. Biol. Eng.*, vol. 9, no. 9, pp. 683–688, 2015.

[61] L. Pothuaud, C. Benhamou, P. Porion, E. Lespessailles, R. Harba, and P. Levitz, "Fractal dimension of trabecular bone projection texture is related to three-dimensional microarchitecture," *J. Bone Mineral Res.*, vol. 15, no. 4, pp. 691–699, 2000.

[62] R. M. Haralick, "On a texture-context feature extraction algorithm for remotely sensed imagery," in *Proc. IEEE Conf. Decis. Control*, 1971, vol. 10, pp. 650–657.

[63] M. Shirvaikar, N. Huang, and X. N. Dong, "The measurement of bone quality using gray level co-occurrence matrix textural features," *J. Med. Imag. Health Inf.*, vol. 6, no. 6, pp. 1357–1362, 2016.

[64] M. M. Galloway, "Texture analysis using gray level run lengths," *Comput. Graph. Image Process.*, vol. 4, no. 2, pp. 172–179, 1975.

[65] J. F. Veenland, "Texture analysis of the radiographic trabecular bone pattern in osteoporosis," Ph.D. dissertation, Dept. Radiology, Erasmus University Rotterdam, Rotterdam, The Netherlands, 1999.

[66] K. I. Laws, "Textured image segmentation," Univ. Southern California, Los Angeles, CA, USA, Tech. Rep. F-33615-76-C-1203, 1980.

[67] M. Rachidi, C. Chappard, A. Marchadier, C. Gadois, E. Lespessailles, and C. L. Benhamou, "Application of Laws' masks to bone texture analysis: An innovative image analysis tool in osteoporosis," in *Proc. 5th IEEE Int. Symp. Biomed. Imag., Nano Macro*, 2008, pp. 1191–1194.

[68] A. K. Mishra, D. Kim, and I. Andayana, "Development of three dimensional binary patterns for local bone structure analysis," in *Proc. IEEE Int. Conf. Bioinf. Biomed. Workshops*, 2011, pp. 1006–1008.

[69] C. Chappard *et al.*, "Anisotropy changes in post-menopausal osteoporosis: Characterization by a new index applied to trabecular bone radiographic images," *Osteoporosis Int.*, vol. 16, no. 10, pp. 1193–1202, 2005.

[70] B. Brunet-Imbault, G. Lemineur, C. Chappard, R. Harba, and C.-L. Benhamou, "A new anisotropy index on trabecular bone radiographic images using the fast Fourier transform," *BMC Med. Imag.*, vol. 5, no. 1, 2005, Art. no. 4.

[71] A. Gaidel and A. Khramov, "Application of texture analysis for automated osteoporosis diagnostics by plain hip radiography," *Pattern Recognit. Image Anal.*, vol. 25, no. 2, pp. 301–305, 2015.

[72] V. Sapthagirivasan, M. Anburajan, and V. Mahadevan, "Bone trabecular analysis of femur radiographs for the assessment of osteoporosis using DWT and DXA," *Int. J. Comput. Theory Eng.*, vol. 5, no. 4, pp. 616–620, 2013.

[73] ISCD Official Positions, 2015. [Online]. Available: https://www.iscd.org/official-positions/2015-iscd-official-positions-adult/

[74] D. Kathirvelu and M. Anburajan, "Prediction of low bone mass using a combinational approach of cortical and trabecular bone measures from dental panoramic radiographs," *Proc. Inst. Mech. Eng., Part H, J. Eng. Med.*, vol. 228, no. 9, pp. 890–898, 2014.

[75] M. G. Roberts, J. Graham, and H. Devlin, "Image texture in dental panoramic radiographs as a potential biomarker of osteoporosis," *IEEE Trans. Biomed. Eng.*, vol. 60, no. 9, pp. 2384–2392, Sep. 2013.

[76] E. Siris, H. Genant, A. Laster, P. Chen, D. Misurski, and J. Krege, "Enhanced prediction of fracture risk combining vertebral fracture status and BMD," *Osteoporosis Int.*, vol. 18, no. 6, pp. 761–770, 2007.

[77] H. Jeong, J. Kim, T. Ishida, M. Akiyama, and Y. Kim, "Computerised analysis of osteoporotic bone patterns using texture parameters characterising bone architecture," *Brit. J. Radiol.*, vol. 86, no. 1021, pp. 1–10, 2013.

[78] C.-L. Benhamou *et al.*, "Fractal analysis of radiographic trabecular bone texture and bone mineral density: Two complementary parameters related to osteoporotic fractures," *J. Bone Mineral Res.*, vol. 16, no. 4, pp. 697–704, 2001.

[79] E. Lespessailles *et al.*, "Clinical interest of bone texture analysis in osteoporosis: A case control multicenter study," *Osteoporosis Int.*, vol. 19, no. 7, pp. 1019–1028, 2008.

[80] K. Harrar and L. Hamami, "An interconnectivity index for osteoporosis assessment using X-ray images," *J. Med. Biol. Eng.*, vol. 33, no. 6, pp. 569–575, 2013.

[81] A. S. El Hassani, M. El Hassouni, L. Houam, M. Rziza, E. Lespessailles, and R. Jennane, "Texture analysis using dual tree M-band and Rényi entropy: Application to osteoporosis diagnosis on bone radiographs," in *Proc. 9th IEEE Int. Symp. Biomed. Imag.*, 2012, pp. 1487–1490.

[82] R. Jennane, J. Touvier, M. Bergounioux, and E. Lespessailles, "A variational model for trabecular bone radiograph characterization," in *Proc. 11th IEEE Int. Symp. Biomed. Imag.*, 2014, pp. 1283–1286.

[83] L. Houam, A. Hafiane, A. Boukrouche, E. Lespessailles, and R. Jennane, "One dimensional local binary pattern for bone texture characterization," *Pattern Anal. Appl.*, vol. 17, no. 1, pp. 179–193, 2014.

[84] K. Zheng and S. Makrogiannis, "Bone texture characterization for osteoporosis diagnosis using digital radiography," in *Proc. 38th Annu. Int. Conf. Eng. Med. Biol. Soc.*, 2016, pp. 1034–1037.

[85] H. Oulhaj *et al.*, "Trabecular bone characterization using circular parametric models," *Biomed. Signal Process. Control*, vol. 33, pp. 411–421, 2017.
[86] H. Oulhaj *et al.*, "Anisotropic discrete dual-tree wavelet transform for improved classification of trabecular bone," *IEEE Trans. Med. Imag.*, vol. 36, no. 10, pp. 2077–2086, Oct. 2017.
[87] A. Singh, M. K. Dutta, R. Jennane, and E. Lespessailles, "Classification of the trabecular bone structure of osteoporotic patients using machine vision," *Comput. Biol. Med.*, vol. 91, pp. 148–158, 2017.
[88] C. Muramatsu *et al.*, "Quantitative assessment of mandibular cortical erosion on dental panoramic radiographs for screening osteoporosis," *Int. J. Comput. Assisted Radiol. Surg.*, vol. 11, no. 11, pp. 2021–2032, 2016.
[89] M. S. Kavitha *et al.*, "Automatic detection of osteoporosis based on hybrid genetic swarm fuzzy classifier approaches," *Dentomaxillofacial Radiol.*, vol. 45, no. 7, 2016, Art. no. 20160076.
[90] C. Bo *et al.*, "Osteoporosis prescreening using dental panoramic radiographs feature analysis," in *Proc. IEEE 14th Int. Symp. Biomed. Imag.*, 2017, pp. 188–191.
[91] S. Majumdar *et al.*, "In vivo assessment of trabecular bone structure using fractal analysis of distal radius radiographs," *Med. Phys.*, vol. 27, no. 11, pp. 2594–2599, 2000.
[92] S. Lee, J. W. Lee, J.-W. Jeong, D.-S. Yoo, and S. Kim, "A preliminary study on discrimination of osteoporotic fractured group from nonfractured group using support vector machine," in *Proc. 30th Annu. Int. Conf. IEEE Eng. Med. Biol. Soc.*, 2008, pp. 474–477.
[93] K. Hatano, S. Murakami, H. Lu, J. K. Tan, H. Kim, and T. Aoki, "Classification of osteoporosis from phalanges CR images based on DCNN," in *Proc. 17th Int. Conf. Control, Autom. Syst.*, 2017, pp. 1593–1596.
[94] R. Paul, S. Alahamri, S. Malla, and G. J. Quadri, "Make your bone great again: A study on osteoporosis classification," 2017, arXiv preprint arXiv:1707.05385.
[95] L. Pothuaud, P. Carceller, and D. Hans, "Correlations between grey-level variations in 2D projection images (TBS) and 3D microarchitecture: Applications in the study of human trabecular bone microarchitecture," *Bone*, vol. 42, no. 4, pp. 775–787, 2008.
[96] B. C. Silva and W. D. Leslie, "Trabecular bone score," *Endocrinol. Metabolism Clinics*, vol. 46, no. 1, pp. 153–180, 2017.
[97] C. Ripamonti, L. Lisi, A. Buffa, S. Gnudi, and R. Caudarella, "The trabecular bone score predicts spine fragility fractures in postmenopausal caucasian women without osteoporosis independently of bone mineral density," *Med. Arch.*, vol. 72, no. 1, pp. 46–50, 2018.
[98] FRAX, 2008. [Online]. Available: https://www.sheffield.ac.uk/FRAX/tool.jsp
[99] FRC, 2012. [Online]. Available: https://riskcalculator.fore.org/
[100] QFracture, 2016. [Online]. Available: www.qfracture.org
[101] Garvan Fracture Risk, 2008. [Online]. Available: www.garvan.org.au/promotions/bone-fracture-risk/calculator
[102] FRACTURE Index, 2001. [Online]. Available: https://reference.medscape.com/calculator/fracture-index-bone-mineral-d ensity
[103] S. Roux *et al.*, "The World Health Organization Fracture Risk Assessment Tool (FRAX) underestimates incident and recurrent fractures in consecutive patients with fragility fractures," *J. Clin. Endocrinol. Metabolism*, vol. 99, no. 7, pp. 2400–2408, 2014.
[104] N. Dagan, C. Cohen-Stavi, M. Leventer-Roberts, and R. D. Balicer, "External validation and comparison of three prediction tools for risk of osteoporotic fractures using data from population based electronic health records: Retrospective cohort study," *BMJ*, vol. 356, Jan. 2017, Art. no. i6755.
[105] J. Hippisley-Cox and C. Coupland, "Derivation and validation of updated QFracture algorithm to predict risk of osteoporotic fracture in primary care in the United Kingdom: Prospective open cohort study," *BMJ*, vol. 344, 2012, Art. no. e3427.
[106] D. Aw *et al.*, "Fracture risk prediction and treatment thresholds using FRAX, Garvan and QFracture in an osteoporosis clinic population," *Age Ageing*, vol. 44, suppl._2, 2015, Art. no. ii13.
[107] D. Black *et al.*, "An assessment tool for predicting fracture risk in postmenopausal women," *Osteoporosis Int.*, vol. 12, no. 7, pp. 519–528, 2001.
[108] E. Hernlund *et al.*, "Osteoporosis in the European Union: Medical management, epidemiology and economic burden," *Arch. Osteoporosis*, vol. 8, no. 1/2, 2013, Art. no. 136.
[109] "Statistics on availability of MRI machines in different countries.," 2016. [Online]. Available: https://www.statista.com/statistics/282401/density-of-magnetic-resonance-imaging-units-by-country/
[110] "Statistics on availability of CT machines in different countries," 2016. [Online]. Available: https://www.statista.com/statistics/266539/distribution-of-equipment-fo r-computer-tomography/
[111] M. Wallander, K. F. Axelsson, A. G. Nilsson, D. Lundh, and M. Lorentzon, "Type 2 diabetes and risk of hip fractures and non-skeletal fall injuries in the elderly: A study from the fractures and fall injuries in the elderly cohort (FRAILCO)," *J. Bone Mineral Res.*, vol. 32, no. 3, pp. 449–460, 2017.
[112] J. Dytfeld and M. Michalak, "Type 2 diabetes and risk of low-energy fractures in postmenopausal women: Meta-analysis of observational studies," *Aging Clin. Exp. Res.*, vol. 29, no. 2, pp. 301–309, 2017.
[113] J. A. Cauley *et al.*, "Risk factors for hip fracture in older men: the osteoporotic fractures in men study (MrOS)," *J. Bone Mineral Res.*, vol. 31, no. 10, pp. 1810–1819, 2016.
[114] M.-L. Pan, L.-R. Chen, H.-M. Tsao, and K.-H. Chen, "Iron deficiency anemia as a risk factor for osteoporosis in Taiwan: A nationwide population-based study," *Nutrients*, vol. 9, no. 6, 2017, Art. no. 616.
[115] A. Oliveira and C. Vaz, "The role of sarcopenia in the risk of osteoporotic hip fracture," *Clin. Rheumatol.*, vol. 34, no. 10, pp. 1673–1680, 2015.
[116] E. A. Lucassen *et al.*, "Poor sleep quality and later sleep timing are risk factors for osteopenia and sarcopenia in middle-aged men and women: The NEO study," *PloS One*, vol. 12, no. 5, pp. 1–17, 2017.
[117] T. P. Ho-Le, J. R. Center, J. A. Eisman, H. T. Nguyen, and T. V. Nguyen, "Prediction of bone mineral density and fragility fracture by genetic profiling," *J. Bone Mineral Res.*, vol. 32, no. 2, pp. 285–293, 2017.
[118] K. P. Chang, J. R. Center, T. V. Nguyen, and J. A. Eisman, "Incidence of hip and other osteoporotic fractures in elderly men and women: Dubbo Osteoporosis Epidemiology Study," *J. Bone Mineral Res.*, vol. 19, no. 4, pp. 532–536, 2004.
[119] A. Schott *et al.*, "Quantitative ultrasound parameters as well as bone mineral density are better predictors of trochanteric than cervical hip fractures in elderly women. Results from the EPIDOS study," *Bone*, vol. 37, no. 6, pp. 858–863, 2005.
[120] G. Albrand, F. Munoz, E. Sornay-Rendu, F. DuBoeuf, and P. Delmas, "Independent predictors of all osteoporosis-related fractures in healthy postmenopausal women: The OFELY study," *Bone*, vol. 32, no. 1, pp. 78–85, 2003.
[121] A. W. Popp, S. Meer, M.-A. Krieg, R. Perrelet, D. Hans, and K. Lippuner, "Bone mineral density (BMD) and vertebral trabecular bone score (TBS) for the identification of elderly women at high risk for fracture: the SEMOF cohort study," *Eur. Spine J.*, vol. 25, no. 11, pp. 3432–3438, 2016.
[122] P. M. Cawthon, M. Shahnazari, E. S. Orwoll, and N. E. Lane, "Osteoporosis in men: Findings from the Osteoporotic Fractures in Men Study (MrOS)," *Therapeutic Adv. Musculoskeletal Disease*, vol. 8, no. 1, pp. 15–27, 2016.
[123] R. Hollaender *et al.*, "Prospective evaluation of risk of vertebral fractures using quantitative ultrasound measurements and bone mineral density in a population-based sample of postmenopausal women: Results of the Basel Osteoporosis Study," *Ann. Rheumatic Diseases*, vol. 68, no. 3, pp. 391–396, 2009.
[124] E. S. Siris *et al.*, "Identification and fracture outcomes of undiagnosed low bone mineral density in postmenopausal women: Results from the national osteoporosis risk assessment," *Obstetrical Gynecol. Surv.*, vol. 57, no. 4, pp. 220–221, 2002.
[125] D. Hans, C. Durosier, J. A. Kanis, H. Johansson, A.-M. Schott-Pethelaz, and M.-A. Krieg, "Assessment of the 10-year probability of osteoporotic hip fracture combining clinical risk factors and heel bone ultrasound: The EPISEM prospective cohort of 12,958 elderly women," *J. Bone Mineral Res.*, vol. 23, no. 7, pp. 1045–1051, 2008.

Authors' photographs and biographies not available at the time of publication.